Conjugated Polymers Based on Benzo[2,1-b :3,4- b']Dithiophene with Low-Lying Highest Occupied Molecular Orbital Energy Levels for Organic Photovoltaics

ARTICLE *in* ACS APPLIED MATERIALS & INTERFACES · JULY 2009

Impact Factor: 6.72 · DOI: 10.1021/am900327n · Source: PubMed

4 AUTHORS:

Shengqiang Xiao
Wuhan University of Technology
49 PUBLICATIONS **1,518** CITATIONS
SEE PROFILE

Andrew Stuart
University of North Carolina at Chapel Hill
17 PUBLICATIONS **1,862** CITATIONS
SEE PROFILE

Shubin Liu
University of North Carolina at Chapel Hill
155 PUBLICATIONS **5,502** CITATIONS
SEE PROFILE

Wei You
University of North Carolina at Chapel Hill
81 PUBLICATIONS **4,354** CITATIONS
SEE PROFILE

Conjugated Polymers Based on Benzo[2,1-*b*:3,4-*b*′]dithiophene with Low-Lying Highest Occupied Molecular Orbital Energy Levels for Organic Photovoltaics

Shengqiang Xiao,[†,‡] Andrew C. Stuart,[†] Shubin Liu,[§] and Wei You*[,†]

Department of Chemistry, University of North Carolina at Chapel Hill, Chapel Hill, North Carolina 27599-3290, State Key Lab of Advanced Technology for Materials Synthesis and Processing, Wuhan University of Technology, Wuhan, People's Republic of China 430070, and Research Computing Center, University of North Carolina at Chapel Hill, Chapel Hill, North Carolina 25599-3420

ABSTRACT Fusing bithiophene units with a benzo moiety, benzo[2,1-*b*:3,4-*b*′]dithiophene (**BDT**), was projected by theoretical calculations to lower the highest occupied molecular orbital (HOMO) energy level of the resulting polymers compared with that of the bithiophene unit, which would enhance the open circuit voltage of bulk heterojunction photovoltaic cells fabricated from **BDT**-based polymers blended with PCBM. The homopolymer of **BDT** (**HMPBDT**) and alternating copolymer of **BDT** with 2,1,3-benzothiadiazole (**PBDT-BT**) were therefore synthesized and fully characterized. Both the homopolymer (**HMPBDT**) and the copolymer (**PBDT-BT**) were experimentally confirmed to have low HOMO energy levels (−5.70 eV for **HMPBDT** and −5.34 eV for **PBDT-BT**). Introducing the acceptor moiety (2,1,3-benzothiadiazole) successfully lowered the optical band gap of the copolymer from 2.31 eV (**HMPBDT**) to 1.78 eV (**PBDT-BT**). Bulk heterojunction photovoltaic devices were fabricated from blends of these structurally related polymers with PBCM to investigate the photovoltaic performances. The optimized device of **HMPBDT**:PCBM (1:3, 180 nm) exhibited an improved open circuit voltage (V_{oc}) of 0.76 V, a short circuit current (J_{sc}) of 0.34 mA/cm^2, and a fill factor (*FF*) of 0.40, offering an overall efficiency of 0.10%. The observed large phase separation of the thin film by AFM and the large band gap were accountable for the small current. The optimized device of **PBDT-BT**:PCBM (1:3, 55 nm) demonstrated a better efficiency of 0.6%, with $V_{oc} = 0.72$ V, $J_{sc} = 2.06$ mA/cm^2, and $FF = 0.42$. The much improved current was attributed to the lower bandgap and better film morphology. However, the low hole mobility limited the thickness of the **PBDT-BT**:PCBM film, making inaccessible the thicker film which would utilize more light and enhance the current. Further improvements are expected if the mobility and film morphology can be improved by the new materials design, together with low band gap and low HOMO energy level.

KEYWORDS: conjugated polymers • solar cell • fullerene • bulk heterojunction • thin film devices • solution processing

INTRODUCTION

As a potential low-cost alternative to mainstream silicon solar cells, organic solar cells based on conjugated polymers has attracted significant research interest over the past few decades. The cost of manufacturing these carbon-based materials is much lower compared with that of crystalline silicon. More importantly, these soft materials are amenable to a low-cost, roll-by-roll printing process. However, the energy conversion efficiency of the most efficient organic solar cells has been stagnant (5−6%) (1), typically achieved through the bulk heterojunction (BHJ) of regioregular poly(3-hexylthiophene) (RR-P3HT) and [6,6]-phenyl C_{61}-butyric acid methyl ester (PCBM) after extensive optimization (2−4). Since P3HT (with a band gap of 1.9 eV) only absorbs up to 22% of the influx photons of solar spectrum (5), low-band-gap materials were expected to harvest more influx photons to further improve the efficiency of organic solar cells. However, BHJ devices made from these low-band-gap materials with PCBM are usually less efficient (<1%), with only a few exceptions which demonstrated decent efficiencies (3−6%) (6−24). Most of them suffer from either (a) unmatched energy levels with regard to PCBM and thereby a low open circuit voltage (V_{oc}) or (b) low hole mobility and unoptimized morphology, leading to a low short circuit current (J_{sc}) and a small fill factor (*FF*); in some cases both (a) and (b) occur.

To further improve the performance of BHJ type organic solar cells, polymers with a small band gap should still be actively pursued to maximize photon absorption and photogenerated current (high J_{sc}). However, the difference between the HOMO energy level of the donor and the lowest unoccupied molecular orbital (LUMO) of the acceptor also needs to be raised to increase the output of V_{oc}, which is

* To whom correspondence should be addressed. E-mail: wyou@email.unc.edu.
Received for review May 14, 2009 and accepted May 26, 2009
† Department of Chemistry, University of North Carolina at Chapel Hill.
‡ Wuhan University of Technology.
§ Research Computing Center, University of North Carolina at Chapel Hill.
DOI: 10.1021/am900327n

essentially determined by the aforementioned energy level difference (25). Therefore, maximizing the overall energy conversion efficiency (η) requires a delicate balance of the band gap and energy levels of both donor and acceptor materials to collaboratively enhance V_{oc} and the J_{sc}. For example, in the prevalent BHJ system in which conjugated polymers are used as the donor and the PCBM is employed as the acceptor, the J_{sc} value has been significantly enhanced by reducing the band gap of polymers on a number of occasions (19, 22, 23). However, the accompanying V_{oc} is relatively small due to the high-lying HOMO energy level of these polymers, a typical characteristic of thiophene-based low-band-gap polymers. It would be ideal if the low band gap and low HOMO energy level could coexist for the donor polymer, which would result in a high J_{sc} and an increased V_{oc}. This challenge calls for new strategies to design new conjugated polymers to be used in the BHJ with PCBM. One such strategy is to employ polycyclic, fused aromatic molecules.

Polycyclic, fused aromatic molecules have rigidly enforced planarity, benefiting more effective π electron delocalization, which provides two advantages in the design of conjugated polymers for organic photovoltaics. First, the HOMO energy level of related polymers can be tuned through varying the fused aromatic moieties within these polycyclics. Second, the improved $\pi-\pi$ interactions between polymer chains in thin solid films would likely enhance the charge carrier mobility. Combining these advantages with donor−acceptor approach to construct low-band-gap polymers, one would be able to design polymers with small band gaps and low HOMO energy levels, as well as high charge carrier mobility, all of which would collectively boost the energy conversion efficiency.

Following these design rationales, we recently demonstrated a series of structurally related conjugated polymers incorporating fused polycyclics for photovoltaic applications (26). The repeating units consist of two modified **di**thiophene units with one of them planarized by bridging **b**enzo (**BDT**), **n**aphtha (**NDT**), and **q**uinoxalino (**QDT**) segments, respectively. The 2,6-(4,4-dioctyl-4*H*-**c**yclo**p**enta)[2,1-*b*;3,4-*b*′]dithiophene (**CPDT**) moieties were introduced as the other bithiophene unit to improve the solubility of resultant copolymers, facilitating the polymer characterization and photovoltaic device fabrications. Relatively high-lying HOMO energy levels were obtained from these alternating copolymers, which resulted in low V_{oc} (0.4−0.6 V) when combined with PCBM in BHJ solar cell devices. However, density functional theory (DFT) calculation of the **BDT** unit implied a much lower HOMO level (*vide infra*) compared with the experimental value of the HOMO level of the alternating copolymer **BDT**-*co*-**CPDT**, which prompted us to further investigate the intrinsic properties of **BDT**-related conjugated polymers.

In this paper, we will present a detailed investigation of a homopolymer (**HMPBDT**) based on the benzo[2,1-*b*:3,4-*b*′]dithiophene (**BDT**) unit with a low-lying HOMO level and a low-band-gap alternating copolymer (**PBDT-BT**) by incorporating the 2,1,3-benzothiadiazole (**BT**) unit (Figure 1).

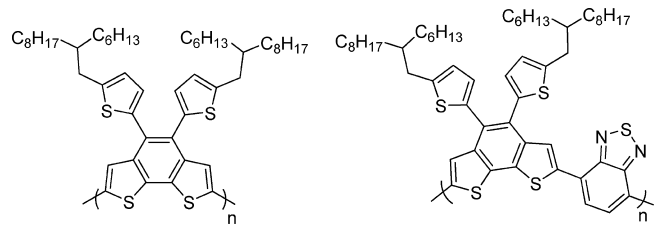

FIGURE 1. Structures of the homopolymer HMPBDT and alternating copolymer PBDT-BT.

HMPBDT indeed showed a much lower HOMO level of −5.70 eV, which translated into a V_{oc} value of 0.76 V in the optimized BHJ devices with PCBM. The HOMO energy level of **PBDT-BT** was determined to be −5.34 eV, leading to a V_{oc} value of 0.72 V in the optimized BHJ devices. The smaller band gap of **PBDT-BT** and better film morphology helped enhance the J_{sc} value from 0.34 mA/cm^2 (in the case of **HMPBDT**) to 2.06 mA/cm^2, resulting an overall efficiency of 0.60% for a BHJ photovoltaic device with a blending ratio of 1:3 (**PBDT-BT**:PCBM) at a thickness of 55 nm.

RESULTS AND DISCUSSION

Monomer Synthesis. Scheme 1 summarizes the synthesis of key monomers, starting from 2-(2-(thiophen-2-yl)ethynyl)thiophene (**1**). Bulky alkyl chains of 2′-octyl-1-dodecyl were readily introduced to 2-(2-(thiophen-2-yl)ethynyl)thiophene to give compound **2** with symmetrically substituted ethyne, which simplified the chemistry in the synthesis of the key building block of benzo[2,1-*b*:3,4-*b*′]dithiophene (**BDT**) via the synthetic protocol in our previous work (26). However, two bulky alkyl chains rendered compound **2** almost insoluble in anhydrous DMF, which resulted in low yields (less than 30%) of precursor monomer **3** through the palladium-catalyzed coupling compound **2** with 3-iodo-2-(3-iodothiophen-2-yl)thiophene. The situation was mitigated by introducing a cosolvent of anhydrous dioxane, which was mixed with anhydrous DMF in a 1:1 ratio to improve the yield to 55%. Trimethyltin chloride was then employed to quench the deprotonated compound **3** (via BuLi) in anhydrous THF to afford the pure distannyl monomer **4** in high yield after a simple workup procedure with no further purification. The iodinated monomer **5** was similarly obtained by the treatment of deprotonated compound **3** with iodine.

Polymer Synthesis. As outlined in Scheme 2, polymers were synthesized by a polycondensation of **4** and corresponding dibrominated and diiodonated comonomers through the Stille coupling reaction according to the conditions described in the Experimental Section. The crude copolymers were washed extensively with water and methanol, followed by Soxhlet extraction with methanol and acetone successively to remove byproducts and oligomers. Finally, the polymers were extracted with hexane, recollected by precipitating them into methanol, and dried under vacuum. The homopolymer **HMPBDT** and alternating copolymer **PBDT-BT** are soluble in common organic solvents such as methylene chloride, chloroform, THF, and toluene

Scheme 1. Synthesis of Monomers

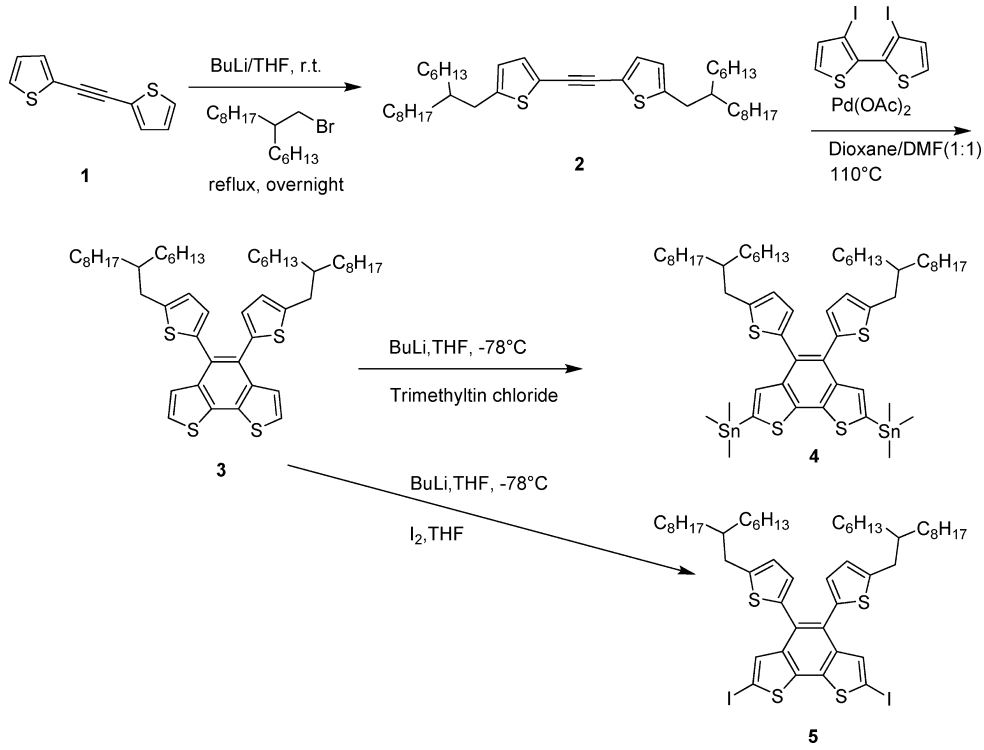

Scheme 2. Synthesis of Polymers HMPBDT and PBDT-BT

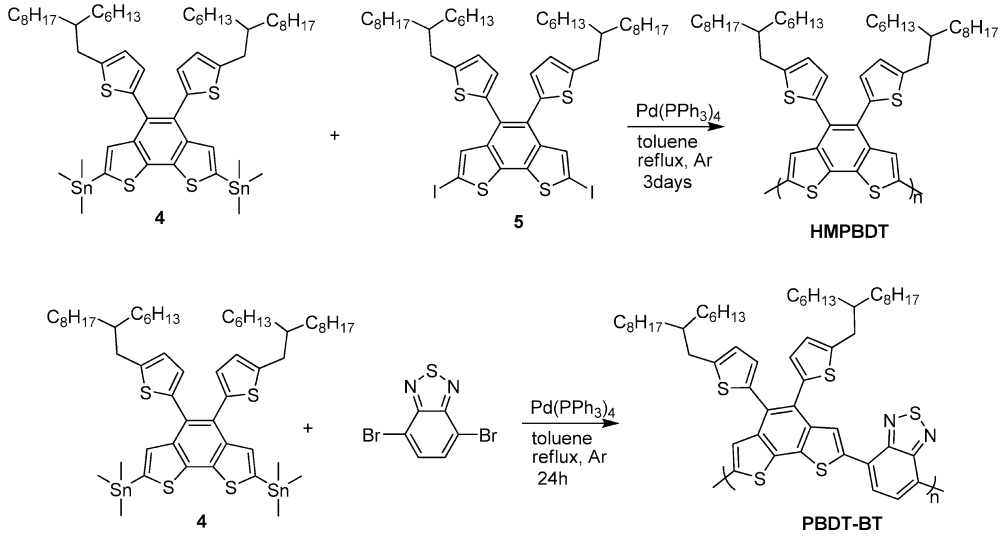

and can be easily processed into thin films for further characterizations. The molecular structures of both polymers were confirmed by ^{1}H NMR spectroscopy (see the Supporting Information).

The yields and molecular weights of polymers are given in Table 1. The molecular weights were determined by gel permeation chromatography (GPC) in THF by referring to polystyrene standards. Both polymers had a high thermal stability with decomposition temperatures over 400 °C under a nitrogen atmosphere, determined from thermogravimetric analysis (TGA). Differential scanning calorimetry (DSC) analysis revealed that both polymers exhibited neither noticeable glass transition nor melting transition (see the Supporting Information).

Table 1. Polymerization Results for Polymers HMPBDT and PBDT-BT

	yield (%)[a]	M_n (kg/mol)[b]	M_w (kg/mol)[b]	PDI[b]	T_d (°C)[c]
HMPBDT	68	11.0	21.5	1.96	402
PBDT-BT	84	10.1	11.9	1.18	400

[a] Soluble polymers extracted with hexane with respect to the overall yield. [b] Determined by GPC in THF using polystyrene standards. [c] The temperature of degradation corresponding to a 5% weight loss determined by TGA at a heating rate of 10 °C/min.

Optical Absorption. The electronic absorption data of both polymers are given in Table 2. All spectroscopic properties were measured both in chloroform solution and as thin films on glass slides. In the case of **HMPBDT**, the

Table 2. Optical and Electrochemical Data of the Polymers HMPBDT and PBDT-BT

	UV−vis abs						cyclic voltammetry		
	$CHCl_3$ soln			film					
polymer	λ_{max} (nm)	λ_{onset} (nm)	E_g (eV)[a]	λ_{max} (nm)	λ_{onset} (nm)	E_g (eV)[a]	E_{onset}^{ox} (V)/ HOMO (eV)	E_{onset}^{red} (V)/ LUMO (eV)	DFT calcd HOMO (eV)
HMPBDT	489, 472	523	2.39	512, 471	540	2.31	0.90/−5.70	−2.15/−2.65	−5.71
PBDT-BT	558	693	1.79	597	703	1.78	0.54/−5.34	−1.64/−3.16	−5.58

[a] Calculated from the intersection of the tangent on the low energetic edge of the absorption spectrum with the abscissa.

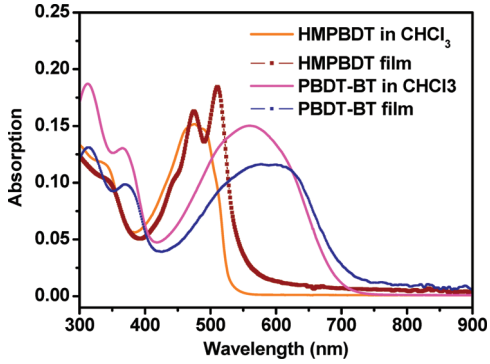

FIGURE 2. UV−vis absorption spectra of HMPBDT and PBDT-BT both in chloroform solution and as thin films.

maximum absorption and the onset absorption wavelengths in the thin film were red-shifted 20 nm compared with those in solution (Figure 2), implying a minimum π stacking in the solid state. Not surprisingly, the homopolymer (**HMPBDT**) exhibited a relatively large band gap around 2.3 eV. The optical absorption spectrum of **PBDT-BT** in the thin film was essentially identical with the measured spectrum in solution, with the former having a small (ca. 30 nm) bathochromic shift of the absorption maximum and the onset. This similarity indicated that only minimum additional π-stacking interactions existed when switching from solution to the thin film. As expected, the band gap of **PBDT-BT** was effectively lowered to 1.78 eV via the alternating donor−acceptor approach (27, 28), which should significantly improve the light harvesting when this polymer is used in photovoltaic (PV) devices.

Electrochemistry. Cyclic voltammograms were recorded from thin films of **HMPBDT** and **PBDT-BT** drop-casted from chloroform solutions as described in the Experimental Section. The potentials were internally calibrated using the ferrocene/ferrocenium redox couple (Fc/Fc^+), which is estimated to have an oxidation potential of −4.8 eV vs vacuum. The CV curves showed reversible oxidations for both polymers. The HOMO energy levels were thus calculated from the onset oxidation potentials (E_{onset}^{ox}), as shown in Table 2. Indeed, the incorporation of benzo[2,1-*b*:3,4-*b*′]dithiophene units into conjugated backbones afforded low-lying HOMO levels of the resulting polymers, corroborating the calculated energy levels (*vide infra*). The low HOMO levels of these donor polymers are essential to achieve large V_{oc} values in PV devices, since V_{oc} is closely correlated to the energy difference between the HOMO of an electron-donor polymer and the LUMO of an electron acceptor. It is worth mentioning that both a low HOMO level and a low band gap were obtained for the copolymer **PBDT-BT**, which would offer improved V_{oc} and enhanced J_{sc}, thereby leading to high efficiency when this polymer is incorporated into a BHJ PV device. The LUMO energy levels of the two polymers were estimated from onset reduction potentials (Table 2).

Theoretical Calculations. Optimized geometries, HOMO and LUMO energy levels, and their electron density distributions for the monomers of **HMPBDT** and **PBDT-BT** were calculated at the B3LYP/6-311+G* level of theory (29, 30) using density functional theory and the Gaussian 03 package (31). To simplify the calculations, all of the alkyl chains were replaced by CH_3 groups. The calculated HOMO energy levels of **BDT** and **BDT-BT** were −5.71 and −5.58 eV, respectively, corroborating experimentally determined values of corresponding polymers (Table 2). For the alternating comonomer **BDT-BT**, the electron density of the HOMO was mainly localized on the **BDT** part (Figure 4), which explains that the low HOMO level of **PBDT-BT** originates from the low

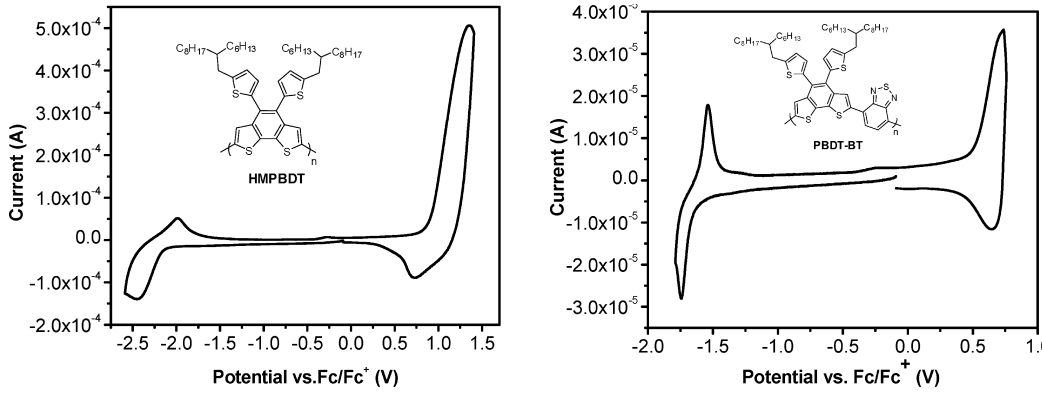

FIGURE 3. Cyclic voltammograms of thin films of HMPBDT and PBDT-BT.

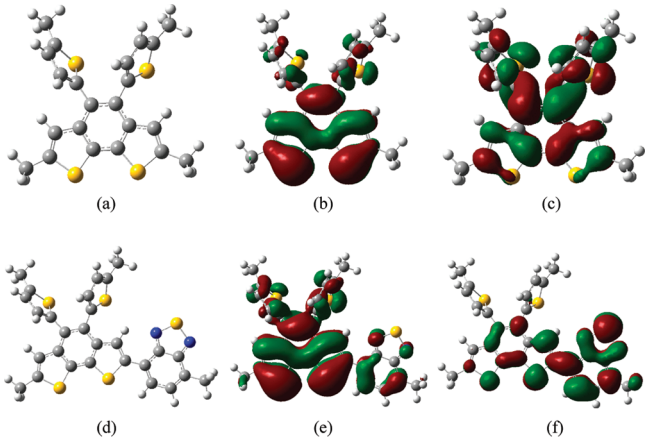

FIGURE 4. Optimized geometry (a), HOMO (b), and LUMO (c) of HMPBDT; (d)−(f) are the respective structures of PBDT-BT.

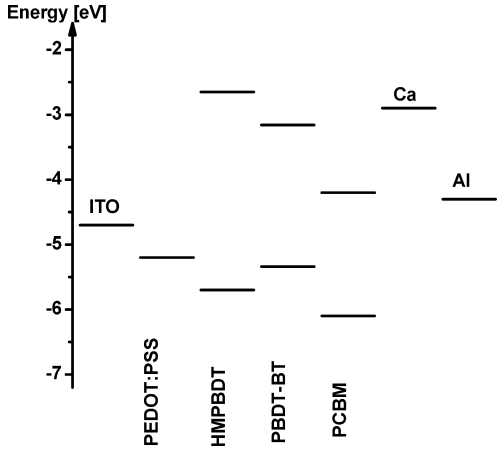

FIGURE 5. Experimental energy diagram with HOMO/LUMO levels of HMPBDT, PBDT-BT, and PCBM in relation to the work functions of the electrode materials ITO/PEDOT:PSS, Ca, and Al in a BHJ photovoltaic device of polymer/PCBM.

HOMO level of the **BDT** unit. Subtly but noticeably, the intramolecular electron transfer between **BDT** and **BT** units caused a slight rise (0.36 eV) of the HOMO level of the donor−acceptor copolymer **PBDT-BT** in comparison with that of the homopolymer **HMPBDT** (Table 2). As indicated in Figure 4f, the electron density of the LUMO was mainly localized on the **BT** unit for the comonomer **BDT-BT**. Thus, the incorporation of the **BT** unit effectively reduced the band gap of **PBDT-BT** due to the very low LUMO energy level of the **BT** unit. These results suggest that judicious combination of different monomers with distinct electronic properties in polymerization could afford low-band-gap polymers with low-lying HOMO levels.

Photovoltaic Properties. Figure 5 gives a diagram of the energy levels of both polymers in relation to that of PCBM and the work functions of indium tin oxide (ITO), poly(3,4-ethylenedioxythiophene) poly(styrenesulfonate) (PEDOT:PSS), calcium (Ca), and aluminum (Al) used as electrodes in an organic PV device. The energy diagram indicated a difference of greater than 0.5 eV between the LUMO energy level of polymers and that of PCBM. This energy level difference provided a sufficient driving force for the directed electron transfer from the photoexcited polymers to PCBM,

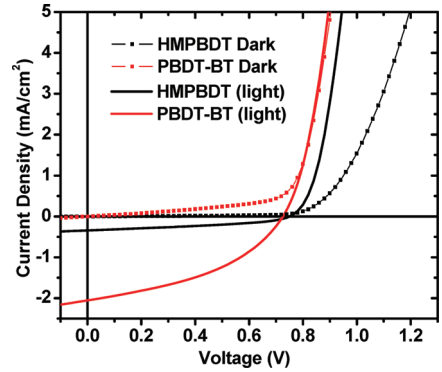

FIGURE 6. Characteristic $I-V$ curves of the optimized devices of HMPBDT and PBDT-BT with and without illumination.

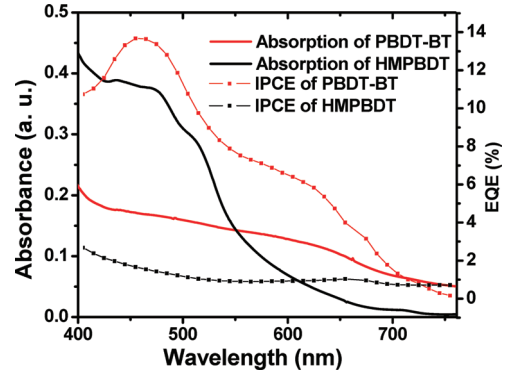

FIGURE 7. IPCE spectra of BHJ photovoltaic devices ITO/PEDOT:PSS (45 nm)/polymer:PCBM (1:3, w/w)/Ca (30 nm)/Al (100 nm) and optical absorptions for the corresponding films of the blends of polymers and PCBM.

which is a prerequisite to observe photovoltaic behavior in a BHJ device of polymer/PCBM.

Photovoltaic properties were investigated in a typical BHJ device configuration: a layer of PEDOT:PSS was spun-cast on top of a prepatterned layer of ITO, followed by a spun-coat layer of the polymer/PCBM blend and a thermally evaporated layer of calcium capped by aluminum as the top electrode. Devices were prepared by varying basic blend properties such as the solvent used, the ratio of polymer to PCBM in the blend solution, and the thickness of thin films to optimize the PV performance. Solar cells were characterized via the widely used practice of illuminating the cells with a calibrated AM 1.5G light source (100 mW/cm^2, 1 Sun), applying a series of voltages, and measuring the current generated between the two electrodes. Devices were typically probed from −0.1 to +1.5 V with illumination and from −0.1 to +2.0 V without illumination. The optimized PV performance characteristics of each polymer solar cell device are given in Table 3, which also includes results from the systematic variation of the film thickness (from the same polymer/PCBM blend).

The characteristically high open circuit voltage (V_{oc}) of **HMPBDT** and **PBDT-BT** (0.76 and 0.72 V, respectively) was indicative of the fused thiophene units bridged by benzene (**BDT**) playing a key role in lowering the HOMO level of the polymers, which was in good agreement with the results from the CV measurements and theoretical calculations. The optimized **HMPBDT** device had a thickness of 180 nm, a J_{sc}

Table 3. Properties of Optimized Solar Cell Devices for HMPBDT and PBDT-BT

polymer	polymer/PCBM	film thickness (nm)	V_{oc} (V)	J_{sc} (mA/cm^2)	*FF*	η (%)	R_S (Ω)	hole mobility (cm^2/(V·s))
HMPBDT	1:3	100	0.76	0.28	0.33	0.07		
HMPBDT	1:3	140	0.70	0.29	0.38	0.08		
HMPBDT	1:3	180	0.76	0.34	0.40	0.10	234	1.58×10^{-4}
PBDT-BT	1:3	55	0.72	2.06	0.42	0.60	121	4.21×10^{-6}
PBDT-BT	1:3	100	0.72	1.39	0.36	0.36		
PBDT-BT	1:3	155	0.70	0.60	0.24	0.10		

value of 0.34 mA/cm^2, and a fill factor of 0.40, together with a V_{oc} value of 0.76 V to yield an overall efficiency (η) of 0.10%. The optimized **PBDT-BT** device had a thickness of 55 nm, a J_{sc} value of 2.06 mA/cm^2, and a fill factor of 0.42, combined with a V_{oc} value of 0.72 V to give an efficiency of 0.60%. Dark current studies were used to calculate the series resistances (RS), which were found to be 234 and 121 Ω for the optimized **HMPBDT** device and the optimized **PBDT-BT** device, respectively.

These optimized devices were subsequently tested for their incident photon to current efficiency (IPCE). In addition, UV−vis measurements were performed on glass substrates which were spun-coat with polymer blends, prepared with the same optimized blend parameters. Both the UV−vis and IPCE curves are shown together (Figure 7) in order to emphasize their correlation. The high absorbance of PCBM in the range of 400−500 nm, associated with its high loading (75 wt % in the blend) with respect to **HMPBDT**, made it difficult to discern the absorption peak from **HMPBDT** (which also absorbs from 400 to 520 nm) in the blend. On the other hand, the extremely thin film thickness (55 nm) of the optimized **PBDT-BT** device diminished the absorption; however, the noticeably high absorption beyond 600 nm was a clear indication of the presence of **PBDT-BT**. The optimized **PBDT-BT** device had a maximum external quantum efficiency (EQE) of 13.7% at 450 nm, while the **HMPBDT** device yielded an EQE of 2.7% at 400 nm, despite the fact that the film thickness of the optimized **PBDT-BT** device was much thinner than that of **HMPBDT** (180 nm).

In order to further understand the different PV performances of these two polymers, the hole mobility of these polymers in the BHJ blends was calculated via the space-charge limited current (SCLC) by constructing optimized devices and replacing the top contact with 40 nm of palladium (see the Experimental Section for more details) (32). Hole mobilities were calculated to be 1.58×10^{-4} and 4.21×10^{-6} cm^2/(V·s) for **HMPBDT** and **PBDT-BT**, respectively. The high hole mobility of **HMPBDT** would allow one to employ a thicker film, which should produce more current due to the improved light absorption as the film thickness increases. In contrast, the much lower hole mobility of **PBDT-BT** would limit the film thickness to a much thinner amount, since the holes would have to transfer a much greater distance in a thicker film, thereby greatly increasing the chances of geminate recombination leading to a reduction in the current. These trends were clearly observed experimentally by correlating measured J_{sc} values with a systematic change of the film thickness (Table 3).

The investigation of the film morphology via AFM on optimized devices provided more insights to explain the significant difference in the efficiencies of **HMPBDT**- and **PBDT-BT**-based PV devices (Figure S5 in the Supporting Information). In comparison with the **PBDT-BT**/PCBM blend, which had a smooth surface (less than 5 nm in roughness) and a relatively good phase separation (less than 100 nm), the **HMPBDT**/PCBM blend showed a much rougher surface (as rough as 50 nm) and a very coarse phase separation (greater than 1 μm). The morphological difference partly explained the much lower J_{sc} and EQE for **HMPBDT** in comparison to those for **PBDT-BT**. The thick film of the **HMPBDT**/PCBM blend absorbed more light (Figure 7), however, as generated excitons would not be able to reach the donor/acceptor interface to generate free charge carriers due to the overly coarse phase separation. Moreover, the larger band gap of **HMPBDT** (2.31 eV) vs that of **PBDT-BT** (1.78 eV) aggravated the low current.

CONCLUSIONS

Fusing bithiophene units with a benzo moiety, benzo[2,1-*b*:3,4-*b*′]dithiophene (**BDT**), was demonstrated by theoretical calculations and experimental results to lower the HOMO energy levels of a resulting homopolymer (**HMPBDT**) and a copolymer with 2,1,3-benzothiadiazole (**PBDT-BT**). The successfully lowered HOMO energy levels translated into high open circuit voltages of BHJ photovoltaic devices fabricated from blends of these polymers with PCBM (**HMPBDT**, 0.76 V; **PBDT-BT**, 0.72 V). The relatively high hole mobility of **HMPBDT** in the BHJ devices allowed the use of a thicker film for better light absorption; however, the nonideal film morphology and large band gap (2.31 eV) rendered a much lower short circuit current (0.34 mA/cm^2). On the other hand, introducing 2,1,3-benzothiadiazole to lower the band gap of **PBDT-BT** was beneficial to the light harvesting, leading to an improved current of 2.06 mA/cm^2. However, the much lower hole mobility of **PBDT-BT** prevented us from using a thicker film to maximize the light absorption (and further enhance the current), thereby limiting the film thickness to 55 nm in the optimized device. These results suggested that only lowering the HOMO energy level and band gap of donor polymers is not enough to achieve higher efficiencies of PCBM-based BHJ photovoltaic devices. High hole mobility and optimized film morphology need to be pursued also in the future materials design, in addition to the low band gap and low HOMO energy level.

EXPERIMENTAL SECTION

Reagents and Instrumentation. All reagents and chemicals were purchased from commercial sources (Aldrich, Acros, Strem, Fluka) and used without further purification unless stated otherwise. Reagent grade solvents were dried when necessary and purified by distillation. Gel permeation chromatography (GPC) measurements were performed on a Waters 2695 Separations Module apparatus with a differential refractive index detector. Tetrahydrofuran (THF) was used as the eluent. Molecular weights were calculated relative to the polystyrene standard. Thermogravimetric analysis (TGA) measurements were carried out on a Perkin-Elmer thermogravimetric analyzer (Pyris 1 TGA) at a heating rate of 10 °C min^{-1} under a nitrogen atmosphere. The temperature of degradation (T_d) is correlated to a 5% weight loss. Differential scanning calorimetry (DSC) analyses were recorded on a DSC220C instrument (SII Seiko Instruments). ^{1}H nuclear magnetic resonance (NMR) measurements were recorded either with a Bruker Avance 300 MHz AMX or Bruker 400 MHz DRX spectrometer. ^{13}C nuclear magnetic resonance (NMR) measurements were carried out with a Bruker 400 MHz DRX spectrometer. Chemical shifts are expressed in parts per million (ppm), and splitting patterns are designated as s (singlet), d (doublet), and m (multiplet). Coupling constants J are reported in hertz (Hz). 2-(2-(Thiophen-2-yl)ethynyl)thiophene (**1**) (33) and 4,7-dibromo-2,1,3-benzothiadiazole (34) were synthesized according to reported procedures.

Electrochemistry. Cyclic voltammetric measurements were carried out using a Bioanalytical Systems (BAS) Epsilon potentiostat equipped with a standard three-electrode configuration. Typically, a three-electrode cell equipped with a glassy-carbon working electrode, a Ag/$AgNO_3$ (0.01 M in anhydrous acetonitrile) reference electrode, and a Pt-wire counter electrode was employed. The measurements were conducted in anhydrous acetonitrile with tetrabutylammonium hexafluorophosphate (0.1 M) as the supporting electrolyte under an argon atmosphere at a scan rate of 100 mV/s. Polymer films were drop-cast onto the glassy-carbon working electrode from a 2.5 mg/mL chloroform solution and dried under a house nitrogen stream prior to measurements. The potential of the Ag/$AgNO_3$ reference electrode was internally calibrated by the ferrocene/ferrocenium redox couple (Fc/Fc^+).

Spectroscopy. UV−visible absorption spectra were obtained by an Agilent Technologies 8453 diode-array spectrophotometer. For the measurements of thin films, polymers were spun-cast onto precleaned glass slides from 10 mg/mL polymer solutions in chlorobenzene.

Polymer Solar Cell Fabrication and Testing. Glass substrates coated with patterned indium-doped tin oxide (ITO) were purchased from Thin Film Devices, Inc. The 150 nm sputtered ITO pattern had a resistivity of 15 Ω/□. Prior to use, the substrates were ultrasonicated for 20 min in acetone followed by deionized water and then 2-propanol. The substrates were dried under a stream of nitrogen and subjected to a treatment of UV−ozone over 30 min. A filtered dispersion of PEDOT:PSS in water (Baytron-PH500) was then spun-cast onto clean ITO substrates at 4000 rpm for 60 s and then baked at 140 °C for 10 min to give a thin film with a thickness of 40 nm. A blend of polymer and PCBM (1:1.6 w/w, 15 mg/mL for polymers) was dissolved in trichlorobenzene with heating at 60 °C for 2 h, filtered through a 0.45 μm poly(tetrafluoroethylene) (PTFE) filter, and spun-cast at 1200 rpm for 60 s onto a PEDOT:PSS layer. The substrates were then dried under vacuum at room temperature for 12 h. The thicknesses of films were recorded by a profilometer (Alpha-Step 200, Tencor Instruments). The devices were finished for measurement after thermal deposition of a 30 nm film of calcium and a 100 nm aluminum film as the cathode at a pressure of $\sim 1 \times 10^{-6}$ mbar. There are eight devices per substrate, with an active area of 12 mm^2 per device. Device characterization was carried out under AM 1.5 G irradiation with an intensity of 100 mW/cm^2 (Oriel 91160, 300 W) calibrated by a NREL certified standard silicon cell. Current versus potential ($I-V$) curves were recorded with a Keithley 2400 digital source meter. IPCE were detected under monochromatic illumination (Oriel Cornerstone 260 $^1/_4$ m monochromator equipped with an Oriel 70613NS QTH lamp), and the calibration of the incident light was performed with a monocrystalline silicon diode. All fabrication steps, after addition of the PEDOT:PSS layer onto an ITO substrate, and characterizations were performed in gloveboxes under a nitrogen atmosphere. For mobility measurements, the hole-only devices in a configuration of ITO/PEDOT:PSS (45 nm)/copolymer−PCBM (1:1.6, w/w)/Pd (40 nm) were fabricated. The experimental dark current densities J of polymer−PCBM blends were measured when applied with voltage from 0 to 6 V. The applied voltage V was corrected from the built-in voltage V_{bi} (35), which was taken as the compensation voltage $V_{bi} = V_{oc} + 0.05$ V, and the voltage drop V_{rs} across the indium tin oxide/poly(3,4-ethylene-dioxythiophene):poly(styrene sulfonic acid) (ITO/PEDOT:PSS) series resistance and contact resistance, which is found to be around 35 Ω from a reference device without the polymer layer. From the plots of $J^{0.5}$ vs V (Supporting Information), hole mobilities of copolymers can be deduced from (36)

$$J = \frac{9}{8}\varepsilon_r\varepsilon_0\mu_h\frac{V^2}{L^3}$$

where ε_0 is the permittivity of free space, ε_r is the dielectric constant of the polymer, which is assumed to be around 3 for the conjugated polymers in our experiment (37), μ_h is the hole mobility, V is the voltage drop across the device, and L is the film thickness of the active layer.

Synthesis. ***2-(2-Hexyldecyl)-5-(2-(5-(2-hexyldecyl)thiophen-2-yl)ethynyl)thiophene (2).*** A 2.5 M n-BuLi solution in hexanes (50 mL, 125 mmol) was added dropwise to an ice bath cooled solution of 11.0 g of 2-(2-(thiophen-2-yl)ethynyl)thiophene (57.9 mmol) in 300 mL of anhydrous THF under argon protection. After it was stirred for an additional 1 h, the reaction mixture was warmed to room temperature and 44.0 g of 2-hexyl-1-bromodecane (144.7 mmol) was added. The mixture was then heated and kept stirring under reflux overnight. After the reaction mixture was cooled to room temperature, 200 mL of water was carefully added into the reaction mixture, resulting in a phase separation. The organic phase was then washed sequentially with brine and water and dried over anhydrous $MgSO_4$. The solvent was removed under reduced pressure. The residue was purified by flash chromatography in hexane to afford 24.0 g of the pure product as a pale yellow liquid (yield 65%). ^{1}H NMR (300 MHz, $CDCl_3$): δ 7.06 (d, 2H, $J = 3.51$ Hz), 6.62 (d, 2H, $J = 3.48$ Hz), 2.71 (d, 4H, $J = 6.54$ Hz), 1.61 (m, 2H), 1.18−1.40 (m, 48H), 0.88 (t, 12H, $J = 6.30$ Hz). ^{13}C NMR (400 MHz, $CDCl_3$): δ 146.95, 131.75, 125.19, 120.69, 85.99, 39.99, 34.58, 33.17, 31.92, 31.89, 29.94, 29.62, 29.34, 26.59, 22.69, 14.10.

***Compound* 3.** To a two-necked round-bottom flask under argon was added 7.1 g (17 mmol) of 3,3′-diiodo-2,2′-bithiophene, 380 mg (1.7 mmol, 10% equiv) of $Pd(OAc)_2$, 27.1 g (42.5 mmol) of compound **2**, 5.7 mL of tributylamine (14.5 g, 51 mmol, 3 equiv). A 30 mL amount of anhydrous dioxane and 30 mL of anhydrous DMF were then added to dissolve the mixture. The mixture was then heated to 130 °C and kept stirring at that temperature for 2 h. After the mixture was cooled to room temperature, 50 mL of ethyl ether was added. The mixture was then washed with a large amount of water, and the organic phase was separated and dried by anhydrous $MgSO_4$. After removal of the solvent under reduced pressue, the viscous residue was further purified by flash chromatography on silica

gel (hexane as eluent) to afford the pure product as a pale yellow liquid (7.5 g, yield 55%). ^{1}H NMR (300 MHz, $CDCl_3$): δ 7.46 (d, 2H, J = 5.42 Hz), 7.37 (d, 2H, J = 5.42 Hz), 6.81 (d, 2H, J = 2.94 Hz), 6.66 (d, 2H, J = 3.18 Hz), 2.74 (d, 4H, J = 6.56 Hz), 1.63 (m, 2H), 1.40−1.20 (m, 48H), 0.92 (m, 12H). ^{13}C NMR (400 MHz, $CDCl_3$): δ 145.15, 138.02, 13785, 133.03, 128.17, 127.65, 125.85, 124.47, 123.86, 39.94, 34.41, 33.22, 31.94, 30.05, 29.71, 29.38, 26.59, 22.70, 14.10.

***Compound* 4.** Compound **3** (0.8 g, 1.0 mmol) was dissolved in dry THF (30 mL) under argon at room temperature. A 2.5 M solution of *n*-BuLi in hexanes (0.84 mL, 2.1 mmol) was then added dropwise. After the mixture was stirred at room temperature for 20 min, trimethyltin chloride (1 M in hexanes, 3 mL, 3 mmol) was injected into the reaction mixture by a syringe. The reaction was then quenched by 20 mL of water after 10 min. The mixture was extracted with ethyl ether. The organic layer was separated, washed with water several times, and dried over anhydrous $MgSO_4$. After solvent removal, the residue was dried under high vacuum to afford 0.8 g of pure product (yield 70%) as a pale yellow viscous liquid. ^{1}H NMR (300 MHz, $CDCl_3$): δ 7.44 (s, 2H), 6.75 (d, 2H, J = 3.06 Hz), 6.62 (d, 2H, J = 3.15 Hz), 2.72 (d, 4H, J = 6.60 Hz), 1.55 (m, 2H), 1.35−1.20 (m, 48H), 0.83−0.88 (m, 12H), 0.40 (s, 18H). ^{13}C NMR (400 MHz, $CDCl_3$): 144.79, 138.81, 138.53, 137.97, 137.35, 133.49, 128.06, 126.73, 124.47, 39.99, 34.46, 33.24, 31.96, 30.11, 29.71, 29.39, 26.62, 22.71, 14.11, 8.25.

***Compound* 5.** Compound **3** (0.8 g, 1.0 mmol) was dissolved in dry THF (30 mL) under argon at room temperature. A 2.5 M solution of *n*-BuLi in hexanes (0.84 mL, 2.1 mmol) was added dropwise. After the mixture was stirred at room temperature for 20 min, 3 g of iodine (3 mmol) previously dissolved in 10 mL of anhydrous THF was transferred into the reaction mixture. The reaction was then quenched by 20 mL of water after 10 min. A 20 mL portion of 5% NaOH solution was added into the mixture,and the solution was stirred for about 10 min. The mixture was then extracted with ethyl ether. The organic layer was separated, washed with water several times, and dried over anhydrous $MgSO_4$. After solvent removal, the residue was purified by flash chromatography on silica gel (hexane as eluent) to afford 0.6 g of pure product (yield 57%) as a pale yellow solid. ^{1}H NMR (300 MHz, $CDCl_3$): δ 7.55 (s, 2H), 6.73 (d, 2H, J = 3.06 Hz), 6.62 (d, 2H, J = 3.15 Hz), 2.70 (d, 4H, J = 6.42 Hz), 1.55 (m, 2H), 1.40−1.20 (m, 48H), 0.88 (m, 12H). ^{13}C NMR (400 MHz, $CDCl_3$): 145.70, 139.07, 136.90, 136.40, 135.39, 128.44, 126.72, 124.57, 75.49, 39.94, 34.41, 33.24, 31.93, 30.04, 29.68, 29.66, 29.36, 26.62, 26.58, 22.68, 14.09.

Synthesis of Polymers via Stille Coupling Polymerization. A representative procedure is as follows. To a 25 mL two-necked round-bottom flask equipped with a condenser was added **4** (452 mg, 0.4 mmol), **5** (421.6 mg, 0.4 mmol), and 20 mL of anhydrous toluene. The mixture was then evacuated and refilled with argon in three cycles to remove oxygen. Then $Pd(PPh_3)_4$ (23 mg, 0.02 mmol, 5% equiv) was added into the reaction flask under an argon stream. The mixture was stirred under reflux for 2 days. After it was cooled to room temperature, the reaction mixture was added dropwise to 100 mL of methanol to obtain precipitates, which were collected by filtration, washed with methanol, and dried. The crude polymer was then extracted subsequently with methanol, acetone, and hexane in a Soxhlet extractor. The fraction from hexane was concentrated under reduced pressure and precipitated into methanol to afford the polymer **HMPBDT** as a yellow solid (440 mg, 68%). ^{1}H NMR (400 MHz, $CDCl_3$): δ 7.55 (2H), 6.82 (4H), 6.68 (2H), 2.75 (4H), 1.64 (4H), 1.50−1.12 (44H), 0.9 (12H).

The polymerization of **PBDT-BT** was carried out at a scale of 0.55 mmol for each monomer. After the reaction, the crude polymer was extracted subsequently with methanol, acetone, and hexane in a Soxhlet extractor. The fraction from hexane was collected under reduced pressure and precipitated into methanol to afford 430 mg of the polymer **PBDT-BT** (yield 84%). ^{1}H NMR (400 MHz, $CDCl_3$): δ 8.36 (2H), 7.63 (2H), 6.82 (4H), 2.81 (4H), 1.80−1.12 (48H), 0.9 (12H).

Acknowledgment. This work was supported by the University of North Carolina at Chapel Hill, the National Science Foundation STC Program at UNC Chapel Hill (No. CHE-9876674), and a DuPont Science and Engineering Grant. We thank Mr. Jeremy Niskala for acquiring AFM images.

Supporting Information Available: Figures giving ^{1}H spectra, TGA and DSC curves of both polymers, AFM images of polymer:PCBM blends, and $J^{0.5}$ vs V plots of mobility measurements of both polymers. This material is available free of charge via the Internet at http://pubs.acs.org.

REFERENCES AND NOTES

(1) Kim, J. Y.; Lee, K.; Coates, N. E.; Moses, D.; Nguyen, T. Q.; Dante, M.; Heeger, A. J. *Science* **2007**, *317*, 222–225.
(2) Li, G.; Shrotriya, V.; Huang, J. S.; Yao, Y.; Moriarty, T.; Emery, K.; Yang, Y. *Nat. Mater.* **2005**, *4*, 864–868.
(3) Ma, W. L.; Yang, C. Y.; Gong, X.; Lee, K.; Heeger, A. J. *Adv. Funct. Mater.* **2005**, *15*, 1617–1622.
(4) Kim, Y.; Cook, S.; Tuladhar, S. M.; Choulis, S. A.; Nelson, J.; Durrant, J. R.; Bradley, D. D. C.; Giles, M.; McCulloch, I.; Ha, C.-S.; Ree, M. *Nat. Mater.* **2006**, *5*, 197–203.
(5) Bundgaard, E.; Krebs, F. C. *Solar Energy Mater. Solar Cells* **2007**, *91*, 954–985.
(6) Zhang, F.; Jespersen, K. G.; Björström, C.; Svensson, M.; Andersson, M. R.; Sundström, V.; Magnusson, K.; Moons, E.; Yartsev, A.; Inganäs, O. *Adv. Funct. Mater.* **2006**, *16*, 667–674.
(7) Andersson, L. M.; Zhang, F.; Inganas, O. *Appl. Phys. Lett.* **2007**, *91*, 071108.
(8) Slooff, L. H.; Veenstra, S. C.; Kroon, J. M.; Moet, D. J. D.; Sweelssen, J.; Koetse, M. M. *Appl. Phys. Lett.* **2007**, *90*, 143506.
(9) Gadisa, A.; Mammo, W.; Andersson, L. M.; Admassie, S.; Zhang, F.; Andersson, M. R.; Inganäs, O. *Adv. Funct. Mater.* **2007**, *17*, 3836–3842.
(10) Mühlbacher, D.; Scharber, M.; Morana, M.; Zhu, Z.; Waller, D.; Gaudiana, R.; Brabec, C. *Adv. Mater.* **2006**, *18*, 2884–2889.
(11) Zhu, Z.; Waller, D.; Gaudiana, R.; Morana, M.; Muhlbacher, D.; Scharber, M.; Brabec, C. *Macromolecules* **2007**, *40*, 1981–1986.
(12) Peet, J.; Kim, J. Y.; Coates, N. E.; Ma, W. L.; Moses, D.; Heeger, A. J.; Bazan, G. C. *Nat. Mater.* **2007**, *6*, 497–500.
(13) Blouin, N.; Michaud, A.; Leclerc, M. *Adv. Mater.* **2007**, *19*, 2295–2300.
(14) Blouin, N.; Michaud, A.; Gendron, D.; Wakim, S.; Blair, E.; Neagu-Plesu, R.; Belletete, M.; Durocher, G.; Tao, Y.; Leclerc, M. *J. Am. Chem. Soc.* **2008**, *130*, 732–742.
(15) Park, S. H.; Roy, A.; Beaupre, S.; Cho, S.; Coates, N.; Moon, J. S.; Moses, D.; Leclerc, M.; Lee, K.; Heeger, A. J. *Nat. Photon.* **2009**, *3*, 297–302.
(16) Wong, W.-Y.; Wang, X.-Z.; He, Z.; Djurisic, A. B.; Yip, C.-T.; Cheung, K.-Y.; Wang, H.; Mak, C. S. K.; Chan, W.-K. *Nat. Mater.* **2007**, *6*, 521–527.
(17) Liu, L.; Ho, C.-L.; Wong, W.-Y.; Cheung, K.-Y.; Fung, M.-K.; Lam, W.-T.; Djurisici, A. B.; Chan, W.-K. *Adv. Funct. Mater.* **2008**, *18*, 2824–2833.
(18) Wu, P.-T.; Bull, T.; Kim, F. S.; Luscombe, C. K.; Jenekhe, S. A. *Macromolecules* **2009**, *42*, 671–681.
(19) Wienk, M. M.; Turbiez, M.; Gilot, J.; Janssen, R. A. J. *Adv. Mater.* **2008**, *20*, 2556–2560.
(20) Chen, C.-P.; Chan, S.-H.; Chao, T.-C.; Ting, C.; Ko, B.-T. *J. Am. Chem. Soc.* **2008**, *130*, 12828–12833.
(21) Wang, E.; Wang, L.; Lan, L.; Luo, C.; Zhuang, W.; Peng, J.; Cao, Y. *Appl. Phys. Lett.* **2008**, *92*, 033307.
(22) Hou, J.; Chen, H.-Y.; Zhang, S.; Li, G.; Yang, Y. *J. Am. Chem. Soc.* **2008**, *130*, 16144–16145.
(23) Liang, Y.; Wu, Y.; Feng, D.; Tsai, S.-T.; Son, H.-J.; Li, G.; Yu, L. *J. Am. Chem. Soc.* **2009**, *131*, 56–57.
(24) Mei, J.; Ogawa, K.; Kim, Y.-G.; Heston, N. C.; Arenas, D. J.; Nasrollahi, Z.; McCarley, T. D.; Tanner, D. B.; Reynolds, J. R.; Schanze, K. S. *ACS Appl. Mater. Interfaces* **2009**, *1*, 150–161.

(25) Mihailetchi, V. D.; Blom, P. W. M.; Hummelen, J. C.; Rispens, M. T. *J. Appl. Phys.* **2003**, *94*, 6849–6854.
(26) Xiao, S. Q.; Zhou, H. X.; You, W. *Macromolecules* **2008**, *41*, 5688–5696.
(27) Havinga, E. E.; Tenhoeve, W.; Wynberg, H. *Synth. Met.* **1993**, *55*–*57*, 299–306.
(28) Roncali, J. *Chem. Rev.* **1997**, *97*, 173–205.
(29) Becke, A. D. *J. Chem. Phys.* **1993**, *98*, 5648–5652.
(30) Lee, C. T.; Yang, W. T.; Parr, R. G. *Phys. Rev. B* **1988**, *37*, 785–789.
(31) Frisch M. J. T., G. W.; Schlegel, H. B.; Scuseria, G. E.; Robb, M. A.; Cheeseman, J. R.; Montgomery, J. A., Jr.; Vreven, T.; Kudin, K. N.; Burant, J. C.; Millam, J. M.; Iyengar, S. S.; Tomasi, J.; Barone, V.; Mennucci, B.; Cossi, M.; Scalmani, G.; Rega, N.; Petersson, G. A.; Nakatsuji, H.; Hada, M.; Ehara, M.; Toyota, K.; Fukuda, R.; Hasegawa, J.; Ishida, M.; Nakajima, T.; Honda, Y.; Kitao, O.; Nakai, H.; Klene, M.; Li, X.; Knox, J. E.; Hratchian, H. P.; Cross, J. B.; Adamo, C.; Jaramillo, J.; Gomperts, R.; Stratmann, R. E.; Yazyev, O.; Austin, A. J.; Cammi, R.; Pomelli, C.; Ochterski, J. W.; Ayala, P. Y.; Morokuma, K.; Voth, G. A.; Salvador, P.; Dannenberg, J. J.; Zakrzewski, V. G.; Dapprich, S.; Daniels, A. D.; Strain, M. C.; Farkas, O.; Malick, D. K.; Rabuck, A. D.; Raghavachari, K.; Foresman, J. B.; Ortiz, J. V.; Cui, Q.; Baboul, A. G.; Clifford, S.; Cioslowski, J.; Stefanov, B. B.; Liu, G.; Liashenko, A.; Piskorz, P.; Komaromi, I.; Martin, R. L.; Fox, D. J.; Keith, T.; Al-Laham, M. A.; Peng, C. Y.; Nanayakkara, A.; Challacombe, M.; Gill, P. M. W.; Johnson, B.; Chen, W.; Wong, M. W.; Gonzalez, C.; Pople, J. A. *Gaussian 03*; revision E.01; Gaussian, Inc., Pittsburgh, PA, 2003.
(32) Mihailetchi, V. D.; Xie, H. X.; de Boer, B.; Koster, L. J. A.; Blom, P. W. M. *Adv. Funct. Mater.* **2006**, *16*, 699–708.
(33) Mio, M. J.; Kopel, L. C.; Braun, J. B.; Gadzikwa, T. L.; Hull, K. L.; Brisbois, R. G.; Markworth, C. J.; Grieco, P. A. *Org. Lett.* **2002**, *4*, 3199–3202.
(34) Mancilha, F. S.; Neto, B. A. D.; Lopes, A. S.; Moreira, P. F.; Quina, F. H.; Goncalves, R. S.; Dupont, J. *Eur. J. Org. Chem.* **2006**, 4924–4933.
(35) Mihailetchi, V. D.; Koster, L. J. A.; Blom, P. W. M.; Melzer, C.; de Boer, B.; van Duren, J. K. J.; Janssen, R. A. J. *Adv. Funct. Mater.* **2005**, *15*, 795–801.
(36) Goodman, A. M.; Rose, A. *J. Appl. Phys.* **1971**, *42*, 2823–2830.
(37) Goh, C.; Kline, R. J.; McGehee, M. D.; Kadnikova, E. N.; Fréchet, J. M. J. *Appl. Phys. Lett.* **2005**, *86*, 122110–122113.

AM900327N